ELSEVIER

Journal of Nuclear Materials 266–269 (1999) 673–678

journal of nuclear materials

Measurement of edge parameters in TEXTOR-94 at the low and high field side with atomic beams

B. Schweer *, M. Brix, M. Lehnen

Institut für Plasmaphysik, Forschungszentrum Jülich GmbH, EURATOM Association, Trilateral Euregio Cluster, D-52425 Jülich, Germany

Abstract

In TEXTOR-94, He-atoms are injected on the low and high field side using a collimating hole structure. Additionally a supersonic He-beam, which has a very low divergence, is mounted on top of the vessel. At all locations the radial emission profiles of three lines are observed with a radial (1.2 mm) and temporal resolution (100 ms) over the whole discharge. The He-atoms are excited by the plasma and the profiles of emission light of two singlet lines and one triplet line are observed simultaneously. A comparison of the measured line intensity ratios with those obtained by a collisional-radiative model delivers the radial profiles of n_e and T_e in the plasma edge. The comparison of edge profiles at different poloidal positions requires a careful alignment procedure in order to resolve asymmetry effects. Time dependent changes of the plasma positions or shape of the plasma cross-section can be identified by the He-beam diagnostic and must be avoided. The edge profiles at the different poloidal locations of TEXTOR-94 are investigated as a function of the central line averaged electron density in ohmic and neutral beam (NBI) heated discharges. T_e and n_e-values at the last closed flux surface between the low and high field side are compared. As a result of a constant magnetic pressure at one radial position the temperature T_e and density n_e are inversely dependent on the central density, but the changes, which are different on the high and low field side, indicate a horizontal asymmetry. © 1999 Elsevier Science B.V. All rights reserved.

Keywords: Collisional-radiative model; Helium beam; In situ, real-time diagnostic; Plasma edge; TEXTOR

1. Introduction

Transport processes determine the profiles of electron density and temperature whereby the plasma wall interaction is influenced. The absolute values and the profiles of n_e and T_e depend on central plasma density, plasma current, toroidal field and auxiliary heating power. The profiles may also react on recycling properties, different wall materials, wall temperatures and impurities (e.g. edge cooling by Ne-injection) [1,2]. The decay lengths of the profiles rise with increasing distance along the magnetic field line to a wall element (limiter) reaching a maximum at the stagnation point [3]. Poloidal asymmetries at the bottom and top of a tokamak are produced by $\mathbf{E} \times \mathbf{B}$ drifts [4] or by a horizontal shift of the plasma position. The typical decay lengths are about 10 mm and the measurement of deviations requires diagnostics with high spatial resolution. The appearance of hot wall elements [5], radiation cooling [6], multifaceted axisymmetric radiation from the edges (MARFEs) [7], mode transitions [1] and plasma turbulence [8–10] influence the T_e and n_e-profiles and may overlay the asymmetry effects. Time dependent measurements are necessary for the identification of machine dependent effects. At TEXTOR-94 saturation of the iron core can produce a small elongation of the plasma in contrast to the usually circular plasma. Sawteeth and NBI-pulses influence the feedback system for horizontal positioning.

In this paper we describe the He-beam diagnostics at TEXTOR-94. A comparison of results obtained at different poloidal positions requires a high accuracy of the radial alignment and intensity calibration which are explained in detail. We analyze measured edge profiles of n_e and T_e at different poloidal positions during the flat

* Corresponding author. Tel.: +49 2461 615536; fax: +49 2461 613331; e-mail: b.schweer@fz-juelich.de

0022-3115/99/$ – see front matter
PII: S0022-3115(98)00836-8

top phase of TEXTOR-94 discharges. Measurements are available at the low and high field side and in a few cases also at the top of TEXTOR-94.

2. Thermal He-beam method

We apply thermal He-beams for the local determination of n_e and T_e-profiles at TEXTOR-94 [11,12]. The line intensity ratios of two transitions in the singlet ($\lambda_1 = 668$ nm, $\lambda_2 = 728$ nm) and one in the triplet system ($\lambda_3 = 706$ nm) of He are measured. The beams are injected into the plasma boundary and the emission profiles are observed nearly perpendicular in order to get the best space resolution. Because of the relatively high electron density in the boundary plasma, a corona like equilibrium cannot describe the line intensities. Therefore, a collisional-radiative model has been developed [13,14]. Population densities of excited levels, which are normalized to the ground state population density, reach a constant value after a certain time. This *relaxation time* depends mainly on n_e. The thermal velocity of the He-atoms is 1.7 km/s. In order to resolve a typical decay length of 5 mm, a relaxation time below 3 μs is necessary. This requires a minimum local edge density of 10^{18} m^{-3}. In case of a sufficient high electron density, T_e and n_e can simply be calculated by comparing measured line intensity ratios with the equilibrium results of the collisional-radiative model.

The model shows that the selected line intensity ratio of λ_2/λ_3 is insensitive to n_e-variation and therefore applied for the determination of T_e. In contrast, the line intensity ratio λ_1/λ_2 is insensitive to T_e-variations and used for the determination of n_e. The accuracy of the model relies on the quality of the rate coefficients. Mainly data, recommended by de Heer et al. [15], which are also provided in the ADAS data base [16], are applied in the model. We have measured the intensities of several other lines (501.6, 504.8, 447.2, 471.3 and 587.6 nm) which were compared with the results from the collisional-radiative model. They agree within an error of ±20% [17]. There exists still a discrepancy for the description of the penetration depth of the thermal He-atoms which is shorter in reality than predicted by the model. Higher ionization rates, cx-processes and proton collision might be the reason for this. The dependence of n_e and T_e on the calculated line intensity ratios is presented in Fig. 1. Electron temperatures below 10 eV lead to increasing errors in the n_e-measurements, because the line intensity ratios are no longer perpendicular to each other.

3. Experimental conditions

TEXTOR-94 is a medium size tokamak with $R_0 = 1.75$ m major and $|R - R_0| = 460$ mm minor radii. Inside the vessel a liner is installed with a radius of 550 mm. The plasma radius is determined by poloidal limiters, which can be retracted, at top, bottom and outboard side of the vessel. At the outward side on the liner, 45° below the equatorial plane, a toroidal belt limiter, ALT II, is installed, which is fixed at 460 mm. Additionally on the high field side at $R - R_0 = -498$ mm a toroidal bumper limiter is mounted on the liner. All limiters are made of carbon. Thermal expansion of in-vessel components has to be taken into account. The liner and vessel temperatures are 300°C and 150°C, respectively. The supporting structure of the poloidal limiter is fixed at the transformer yokes of TEXTOR-94 and does therefore not move when the vessel is heated. The ALT II limiter moves outward with increasing temperature. At a liner temperature of 300°C with retracted poloidal limiters, the radius of the last closed flux surface (LCFS) is at $|R - R_0| = 463$ mm. The radial movement of the liner of 5 mm reduces the distance between the LCFS and the bumper limiter to 30 mm. The results presented here were obtained in a deuterium plasma after siliconization of the wall and limiter [18,19]. The plasma current, I_p, was mainly 350 kA and the line averaged central electron density, $\bar{n}_e(0)$, was increased from 1.5×10^{19} to 5.5×10^{19} m^{-3}, respectively. Ohmically and NBI heated discharges were investigated.

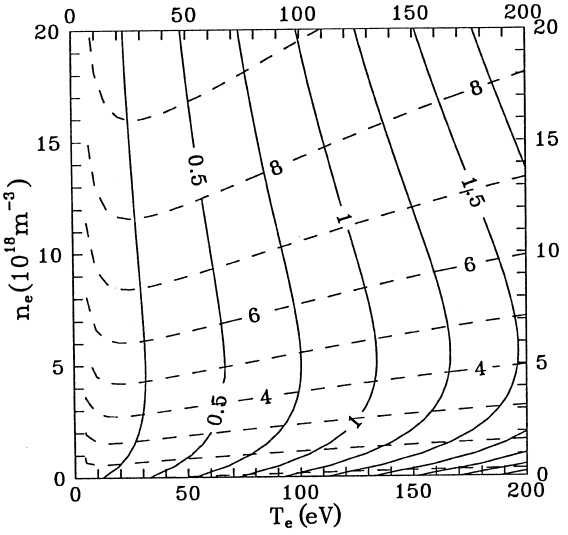

Fig. 1. Calculated line intensity ratios as a function of n_e and T_e in the collisional-radiative model for stationary conditions. I (667.8 nm)/I (728.1 nm) (dashed lines) is used for determination of n_e (insensitive to T_e), I (728.1 nm)/I (706.5 nm) (solid lines) is used for determination of T_e (insensitive to n_e).

4. Experimental set-up

At TEXTOR-94 thermal He-beams are installed at the low field (LFS) and high field side (HFS) in the

equatorial plane and on top of the vessel but at different toroidal positions. A schematic view of the beams in a poloidal cross-section is given in Fig. 2. A flux of about 2×10^{18} He-atoms/s is produced by effusive sources at the LFS and HFS. The collimating hole structure on the LFS is located at liner position and the LCFS is about 90 mm apart. On the HFS the beam is mounted in a tile of the bumper limiter. In both beams the neutral He-density is about 1×10^{16}–1×10^{17}m^{-3} in the maximum of emission. A supersonic He-beam is installed on top of TEXTOR-94. The source is installed far away (0.7 m) from the LCFS. The flux is only $\approx 5 \times 10^{16}$ He-atoms/s, but the beam has a very low divergence (±1°), and the neutral density in the plasma edge is comparable to that of the effusive sources. The lower amount of injected He leads to a reduction of background light from recycled He. This is very important, when several beams are applied at different locations in the tokamak.

All He-beams are observed with a spatial resolution of $\leqslant 1.2$ mm in the radial direction. Dependent on the accessible windows, different detection systems are applied at the individual beams. At the low field side each wavelength is selected by a narrow bandwidth interference filter (1 nm FWHM) and imaged on a multichannel plate (MCP) with individual linear diode arrays. Due to the rectangular shape (1:10) of the pixels the light is integrated over 12 mm in toroidal direction. The He-beam at the high field side can only be observed through a small window which does not allow the installation of the similar three channel observation system. Therefore the light is imaged onto a spectrometer slit. At the exit plane the spectra from 660 to 750 nm (spectral resolution $= 0.7$ nm/pixel) over a radial range of 70 mm are recorded via a 2d-camera with MCP. The optimal width of the entrance slit of 60 μm is determined by the pixel size but limits the integration width in vertical direction to only 0.6 mm. The same camera system is used for the observation of the supersonic beam. The wavelength selection is done by narrow bandwidth interference filters. Therefore still three identical discharges are needed for the measurements of the T_e and n_e-profiles. The 2d-camera was selected since the narrow extension of the supersonic He-beam allows the simultaneous observation of the background light in a toroidally shifted volume.

Background light from recycled He or from the plasma itself can have some influence on the evaluation of the edge profiles. For technical reasons gating and chopping is only possible for the supersonic beam but not for the effusive sources. In Fig. 3 the measured radial profiles of the emission lines at λ_1, λ_2 and λ_3 on the LFS are presented. Some signals have still a significant value at $R - R_0 < 400$ mm where the beam should already be completely ionized. This background, resulting mainly from higher ionized impurity lines, is dependent on the plasma conditions and drops nearly to 0 at the LCFS. A good approximation for subtraction of the background light is a straight line, starting at the measured value at the smallest radius and leading to 0 at $R - R_0 = 470$ mm (dashed line). The horizontal part represents the dark current of the array.

The spectra obtained from the He-beam at the high field side could not be evaluated in the same way for background subtraction. In Fig. 4 the typical spectrum at the LCFS of the inner He-beam is shown. Inside the plasma the radial profiles are similar to those obtained at the low field side. In the scrape-off-layer (SOL), there is a large contribution from light emissions of recycled atoms from the near bumper limiter. Therefore at every radial position the background light determined at the wings of the He-lines is subtracted.

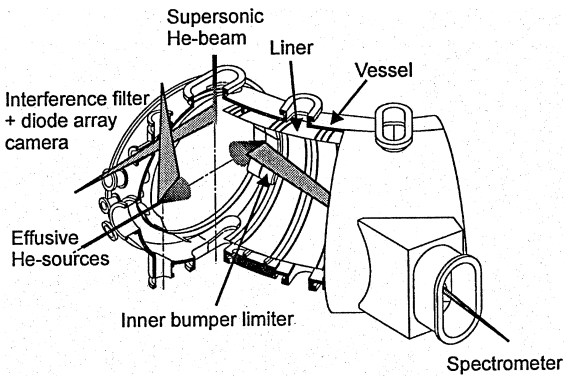

Fig. 2. Schematic view of the He-beam locations in a poloidal cross-section and the appropriate observation systems. The beams at TEXTOR are located at different toroidal positions.

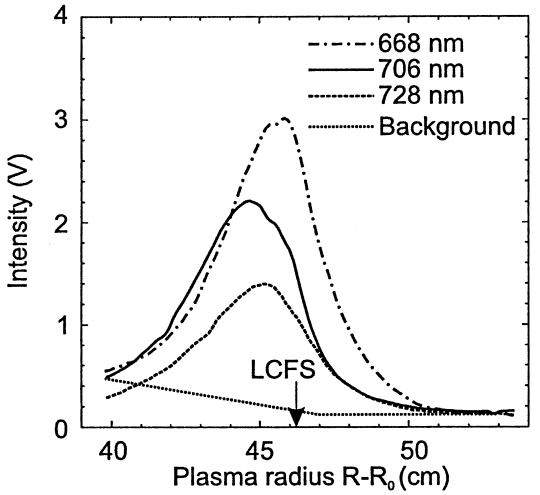

Fig. 3. LFS: radial profiles of the line intensities at $\lambda_1 = 667.8$ nm, $\lambda_2 = 728.1$ nm and $\lambda_3 = 706.5$ nm. The dotted line represents the subtracted intensity of background light.

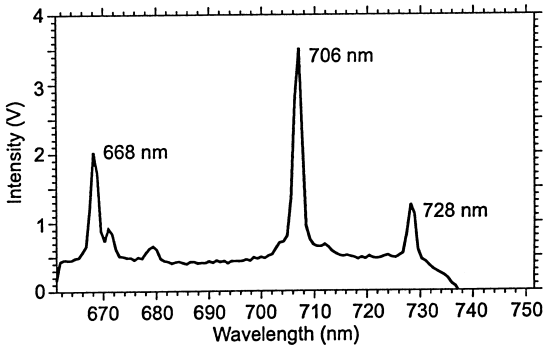

Fig. 4. HFS: spectral intensity profile of He at the LCFS.

The optical transmission and spectral sensitivity of the observation systems were calibrated at all three wavelengths with a halogen lamp inside the tokamak which was cross-calibrated with a tungsten ribbon lamp.

For the interpretations of the asymmetries one has to identify the magnetic surface which is crossed by the beams. In fact all local calibrations are deduced from the mechanical structure and performed under vacuum conditions in presence of a heated liner and vessel. At the LFS an illuminated slit can be moved into the observation volume for the alignment of the detection system. The supporting structure of the slit is fixed with respect to the toroidal field coils. Therefore the absolute radial position is known with an accuracy of ±1.2 mm. The same procedure is applied on top of the vessel, but the transport system follows the thermal expansion of the vessel with +3 mm. The relative accuracy is the same as at the LFS. At the HFS a different calibration method is used. The spectrometer slit is back illuminated into the vessel. The He-beam enters the plasma through a hole in the bumper limiter which is the tangential point of the observation axis. If the light just hits the collimating hole structure, the relative calibration is known from the imaging factor within an error of ±1 mm. The bumper limiter, mounted on the liner, moves 5 mm outwards with the higher vessel temperature.

5. Results and discussion

Asymmetries of the plasma can also be caused by horizontal and vertical shifts of the plasma column. The position signals for the TEXTOR-94 feedback system are delivered from the multichannel HCN-interferometer or from probing coils for the magnetic field mounted outside the liner. The first method compares the line integrated signals at two horizontally symmetric positions, but has to consider the Shafranov shift. The absolute positioning can be done with an accuracy of ±2 nm. This absolute value cannot be reached by the magnetic system. Therefore, to calibrate the zero position, the emission of H_α-light in front of the top and bottom poloidal limiter is compared. Flux changes caused by a vertical plasma shift of ±2 mm can be resolved. This calibration method might lead to a wrong interpretation of asymmetries caused by drift effects. Here a careful analysis of the radial profiles and decay lengths, which can be smaller than 10 mm, is necessary. At the given temperature of liner and vessel the error bar is (−2/+4) mm for determination of the absolute radial positions. The absolute values of electron temperatures and densities were determined with an accuracy of ±20%.

Edge parameters are measured by He-beam diagnostics for various plasma conditions. As an example the time traces of central and local plasma parameters are presented in Fig. 5 for an ohmic heated discharge. The plasma current and density [Fig. 5(a)] were changed stepwise. The temporal development of the electron temperature T_e and density n_e at the LCFS ($R - R_0 = 463$ mm, LFS) and their corresponding decay lengths λ_{n_e}, λ_{T_e} in the SOL is shown in Fig. 5(b) and (c).

In order to take advantage of the full flux swing in the transformer of TEXTOR-94, the power supply has to change polarity at $t \approx 3$ s (dependent on discharge voltage). The iron core is driven into saturation again after (100–200) ms. A drop of n_e and T_e at the LFS and HFS and an increase on top indicates an elongation of the plasma in vertical direction in the range of 2–4 mm. This is also seen by an increase of the H_α-light at the vertical poloidal limiters. Since the decay lengths are in the range of 10 mm, the fluxes in the plasma boundary will be influenced. As a consequence, asymmetry measurements at TEXTOR-94 should be performed in the first part of the discharges.

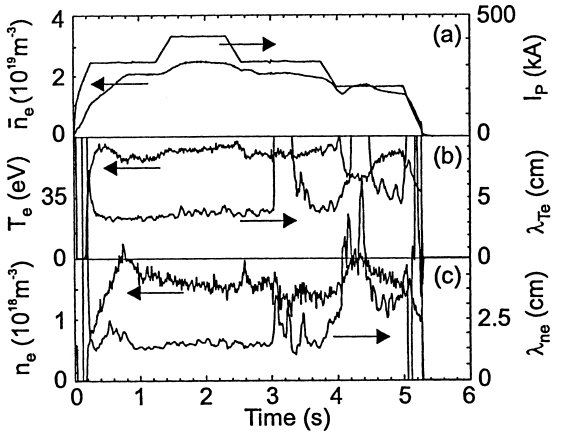

Fig. 5. Temporal development of central and edge (LFS) plasma parameter (# 77536). (a) Line averaged central electron density and plasma current, (b) electron temperature at the LCFS and corresponding decay length and (c) electron density at the LCFS and corresponding decay length.

The temperature rise in the edge at $t = 1.3$ s is connected with an increase of the plasma current from 300 to 450 kA. The gradient in the SOL flattens. This is indicated by the small increase of λ_{T_e}. Even with an increase of the central electron density the edge density falls slightly which might be caused by a better confinement or a change in the safety factor q. The larger λ_{n_e} might be an effect of the higher central density. Asymmetries should be investigated during the flat top phase with constant core parameter.

The radial profiles of n_e (Fig. 6) and T_e (Fig. 7), which are obtained at three poloidal beam positions in the same discharge, are measured during the flat top phase at 1 s. The line averaged central density was 3×10^{19} m^{-3}. Although the alignment procedure has been applied, the profiles are different at the three poloidal positions. The explanation of this effect by only plasma shifts can be excluded. The higher n_e and lower T_e on the HFS might be influenced by the small distance to the bumper limiter which acts as a particle source. Qualitatively the same development of asymmetries in the plasma profiles could be explained by model calculations with a 2d-two fluid-code SOLXY which considers the role of drift motions [4].

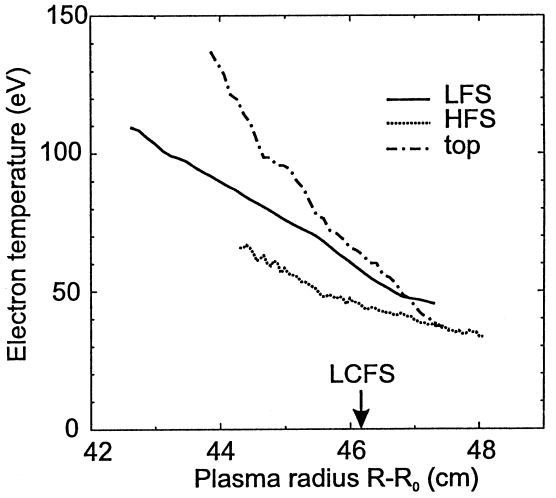

Fig. 6. Radial profiles of n_e at the three poloidal positions for $t = 1.0$ s (# 77536).

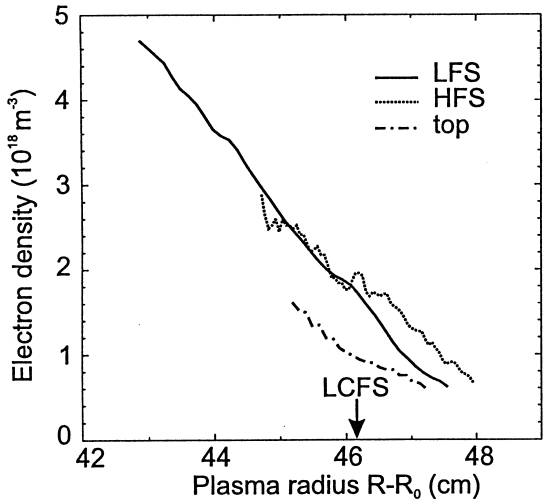

Fig. 7. Radial profiles of T_e at the three poloidal positions for $t = 1.0$ s (# 77536).

The results presented in this section were selected after a careful selection procedure for the plasma positioning. The dependence of the edge parameters at the LCFS on $\bar{n}_e(0)$ for ohmic and NBI (1.2 ± 0.2) MW heated plasmas is presented in Fig. 8 for LFS and Fig. 9 for HFS. The discharge current was 350 kA. The solid lines indicate the best fits in respect to $\bar{n}_e(0)$. The dotted lines represent constant $\bar{n}_e(0)$-values. In all discharges the temperature at the LCFS never falls below 45 eV. With additional heating the operational range was extended, for the selected power up to about 1×10^{19} m^{-3}, but then a MARFE occurred. Since the MARFEs, arising at the HFS [7], lead to very low temperatures (few eV) and high densities (3×10^{20} m^{-3}), the edge data for this case are only available for the LFS in Fig. 8. Moving the plasma inward decreases the density limit for the MARFE, whereas a shift outward allows higher density operation [7]. The reason might be the change of recycling at the bumper limiter.

At the HFS the data base is much smaller. For NBI-heated discharges the lowest temperature at the LCFS is about 30 eV. In comparison to the LFS, the local electron densities are higher and the temperatures are lower

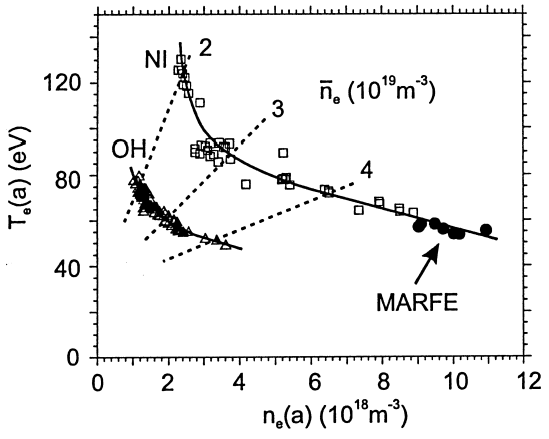

Fig. 8. LFS: dependence of T_e and n_e at the LCFS on the line averaged central electron density in ohmic and NBI-heated discharges ($I_p = 350$ kA, $P_{NBI} = 1.2$ MW). The solid lines represent the best fits. The dotted lines indicate discharges with similar $\bar{n}_e(0)$.

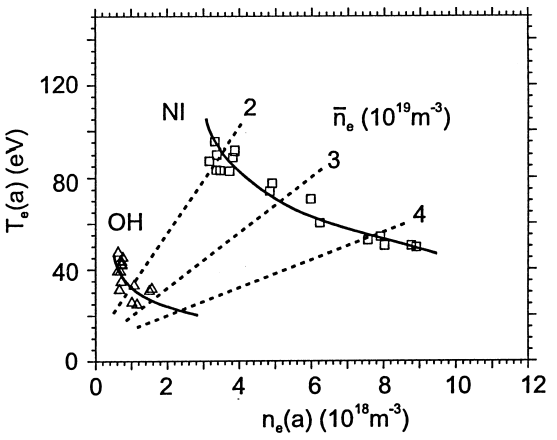

Fig. 9. HFS: Dependence of T_e and n_e at the LCFS on the line averaged central electron density in ohmic and NBI-heated discharges ($I_p = 350$ kA, $P_{NBI} = 1.2$ MW). The solid lines represent the best fits. The dotted lines indicate discharges with similar $\bar{n}_e(0)$.

at the HFS at same $n_e(0)$. The values for the ohmic discharges are significantly lower but the results might already be influenced by the relaxation time of the He-atoms. For the NBI heated discharges a horizontal asymmetry of the edge profiles obviously exists on the HFS and LFS.

6. Summary

He-beam diagnostic is a powerful tool for the determination of T_e and n_e-profiles and of decay lengths in the SOL. The investigation of poloidal asymmetry requires careful alignment procedures for the positioning of the plasma which of course can be done by the He-beam diagnostic. Effects caused by movement or shift of the plasma position, Shafranov shift and deformation of the circular cross-section can also produce asymmetries on the edge profiles. They have to be distinguished from effects produced by drift motions. The measured profiles are qualitatively in agreement with fluid model calculations (2d-two fluid-code SOLXY). At TEXTOR-94 a wide range of plasma densities for 350 kA-discharges was investigated. The temperatures at the LCFS never fall below 45 eV (LFS) and 30 eV (HFS). At densities above 10^{19} m^{-3} MARFEs occurred on the HFS. In all discharges the electron density at the LCFS is higher at the HFS than at the LFS. The electron temperature shows the opposite dependence.

References

[1] B. Unterberg, A.M. Messiaen, J. Ongena et al., Plasma Phys. Contr. Fusion 39 (1997) B189–B206.
[2] P.C. Stangeby, G.M. McCracken, Nucl. Fusion 30 (1990) 1225.
[3] U. Samm, P. Bogen, H. Hartwig et al., J. Nucl. Mater. 162–164 (1989) 24.
[4] H. Gerhauser, H.A. Claassen, Contr. Fusion and Plasma Phys., Proc. Euro. Conf. (Lisboa) 17C (1993) 4–71; H. Gerhauser, H.A. Claassen, J. Nucl. Mater. 176&177 (1990) 721.
[5] A. Pospieszczyk, V. Philipps, E. Casarotto et al., J. Nucl. Mater. 241–243 (1997) 833.
[6] B. Unterberg, M. Brix, R. Jaspers et al., these Proceedings.
[7] U. Samm, M. Brix, F. Durodier et al., these Proceedings.
[8] C. Hidalgo, Plasma Phys. Control. Fusion 37 (1995) A53.
[9] S. Coda, M. Porkolab, Contr. Fusion and Plasma Phys., Proc. Euro. Conf. (Berchtesgarden) 21A (Part 3) (1997) 1141–1144.
[10] A. Huber, PhD thesis, Report Ju1-3422 ISSN 0944–2952 (1997).
[11] B. Schweer, Contr. Fusion and Plasma Phys. Proc. Euro. Conf. (Berlin) 15C (Part IV) (1991) 361–364.
[12] E. Hintz, B. Schweer, Plasma Phys. Contr. Fusion 37 (1995) A87.
[13] B. Brosda, PhD thesis, Ruhr-Universitat Bochum, 1993.
[14] M. Brix, Contr. Fusion and Plasma Phys., Proc. Euro. Conf. (Berchtesgarden) 21A (Part IV) (1997) 1837.
[15] F.J. de Heer, R. Hoekstra, A.E. Kingston, H.P. Summers, Atomic Plasma–Material Interact. Data Fusion 3 (1992) 19; F.J. de Heer, I. Bray et al., Atomic Plasma Material Interact. Data Fusion 6 (1995) 7.
[16] H.P. Summers, M. von Hellermann, Atomic and plasma-material interaction processes in, in: R.K. Janev, H.W. Drawin (Eds.), Contr. Thermonuclear Fusion, Elsevier, Amsterdam, 1993, pp. 87–117.
[17] M. Brix, PhD thesis, Report Jul., to be published.
[18] J. Winter, H.G. Esser et al., Phys. Rev. Lett. 71 (1993) 1549.
[19] J. Ongena, A.M. Messiaen, G. Van Wassenhove et al., Control. Fusion and Plasma Phys., Proc. Euro. Conf. (Lisboa) 17C (Part 1) (1993) I-127.